Heliyon 8 (2022) e09533

Contents lists available at ScienceDirect

Heliyon

journal homepage: www.cell.com/heliyon

Research article

# A comparative evaluation of antibacterial activities of imidazolium-, pyridinium-, and phosphonium-based ionic liquids containing octyl side chains

Rabia Hassan [a], Muhammad Asad Asghar [a], Mudassir Iqbal [a,*], Arshemah Qaisar [b], Uzma Habib [b], Bashir Ahmad [c]

[a] Department of Chemistry, School of Natural Sciences (SNS), National University of Sciences & Technology (NUST), H-12, Islamabad, 44000, Pakistan
[b] Research Center for Modeling and Simulation (RCMS), National University of Sciences & Technology (NUST), H-12, Islamabad, 44000, Pakistan
[c] Department of Biological Sciences, International Islamic University, Islamabad, Pakistan

## GRAPHICAL ABSTRACT

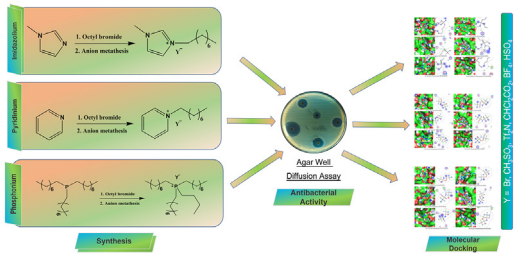


## ARTICLE INFO

*Keywords:*
Imidazolium
Pyridinium
Phosphonium
Ionic liquids
Octyl
Antibacterial activity

## ABSTRACT

Antibacterial activity is an essential property of ionic liquids. In this work, a comprehensive study has been performed on the antibacterial activity of ionic liquids to be utilized for further research and applications. Eighteen ionic liquids *viz.* Octyl Imidazolium, octyl Pyridinium, quaternary phosphonium-based cations containing bromide, sodium methane sulphonates, bis(trifluoromethane sulfonyl) imide, dichloroacetate, tetrafluoroborate, hydrogen sulfate were prepared and characterized with the help of different spectroscopic techniques. All these samples of ionic liquids were tested for their antibacterial activity against the most commonly occurring bacteria in the environment, i.e., *Enterobacter aerogenes (E. aerogenes), Proteus vulgaris (P. vulgaris), Klebsiella pneumoniae (K. pneumoniae), Pseudomonas aeruginosa (P. aeruginosa), Escherichia coli (E. coli), and Streptococcus pyogenes (S. pyogenes)*. Most of the ionic liquids show good antibacterial properties, and imidazolium-based ionic liquids were even more antibacterial as compared to positive control. It was observed that a unique combination of cation and anion is essential to achieve desired antibacterial properties. The mechanism of antibacterial activity was further investigated using density functional theory calculations. A good correlation was found between experimental and theoretical studies.

* Corresponding author.
*E-mail address:* mudassir.iqbal@sns.nust.edu.pk (M. Iqbal).

https://doi.org/10.1016/j.heliyon.2022.e09533
Received 2 February 2022; Received in revised form 14 March 2022; Accepted 19 May 2022

## 1. Introduction

The Healthcare community faces the major challenge of an enhanced number of deaths in hospitalized patients due to microbial infections [1]. These increasing numbers of microbial infections have now gained the attention of researchers worldwide, as evident from the growing number of publications on microbial resistance and its effects on the health of the human population [2]. Bacterial infections can be controlled by sanitization [3], sterilization [4], and by the use of biocides, but the bacteria have developed resistance against them. For example, *E. coli* is responsible for both complicated and uncomplicated UTIs. But, some German populations have developed resistance against cotrimoxazole, which was once used as the first line of defense against UTIs [5].

Ionic liquids (ILs) with inherent antimicrobic properties and tunable nature have now emerged as active pharmaceutical ingredients (API) [6, 7, 8]. ILs mainly consist of an organic cation like imidazolium, pyridinium, quaternary ammonium, and phosphonium which can be combined with various anions to form a diverse set of molecules with distinct properties which can be further changed by the functionalization of either cation or anion [9]. The length of alkyl side chains of ILs directly affects the cytotoxicity, interaction with bovine serum albumin, and toxicity for microbial growth [10]. ILs possess unique physicochemical properties like high viscosity and density as compared to water [11], reduced biodegradability [12], low melting point (<100 °C) [9, 13], high thermal, chemical, and electrochemical stability [11, 14, 15, 16], non-volatile [17], low toxicity [6] solubility in most of the solvents and negligible vapor pressure [18].

Due to their distinctive properties ILs have drawn considerable research interest. The applications of ILs includes antibiofilm [19, 20, 21], anti-corrosion [22, 23], separation [24, 25, 26, 27, 28, 29, 30], bio-catalysis [31], drug delivery [32, 33] and electrochemistry [34]. Several type of ILs are being studied for their antibacterial properties. Some major classes include, 1-butyl-1-methylpyrrolidinium trifluoromethyl sulfonate [22], octyl and hexyl imidazolium bromide [1], -alkyl-vinyl imidazolium bromide monomer and polymer [35], butylimidazolium bromide [36], cinnamyl imidazole [37], pyridinium-based ILs [18, 38], novel phenethyl imidazolium-based ILs [39], amino thiazolyl-functionalized phosphonium ILs [40], quaternary ammonium-based ILs [41] and those derived from choline and geranate [17].

This work reported the synthesis and characterization of pyridinium, phosphonium, and imidazolium-based ionic liquids with different anions. This study compares the effect of different cations containing octyl side chains on antibacterial activity. These ionic liquids were tested for antibacterial activity against *S. pyogenes, E. coli, K. pneumoniae, E. aerogenes, P. vulgaris, P. aeruginosa.* The ILs based on imidazolium show better antibacterial activity than all other tested cations.

## 2. Experimental

### 2.1. Materials and instrument

All analytical grade reagents were used without modifications during the synthesis. The chemicals used included, 1-methylimidazole (DAEJUNG, >99%), pyridine (Sigma-Aldrich, ~99%), tri-octyl phosphine (MACKLIN, 92.23%), octyl bromide (MACKLIN, >95%) methane sulphonic acid (Sigma-Aldrich, 99%), dichloroacetic acid (Sigma-Aldrich, >98%), potassium hydrogen sulfate (MERCK, 35–37%), lithium

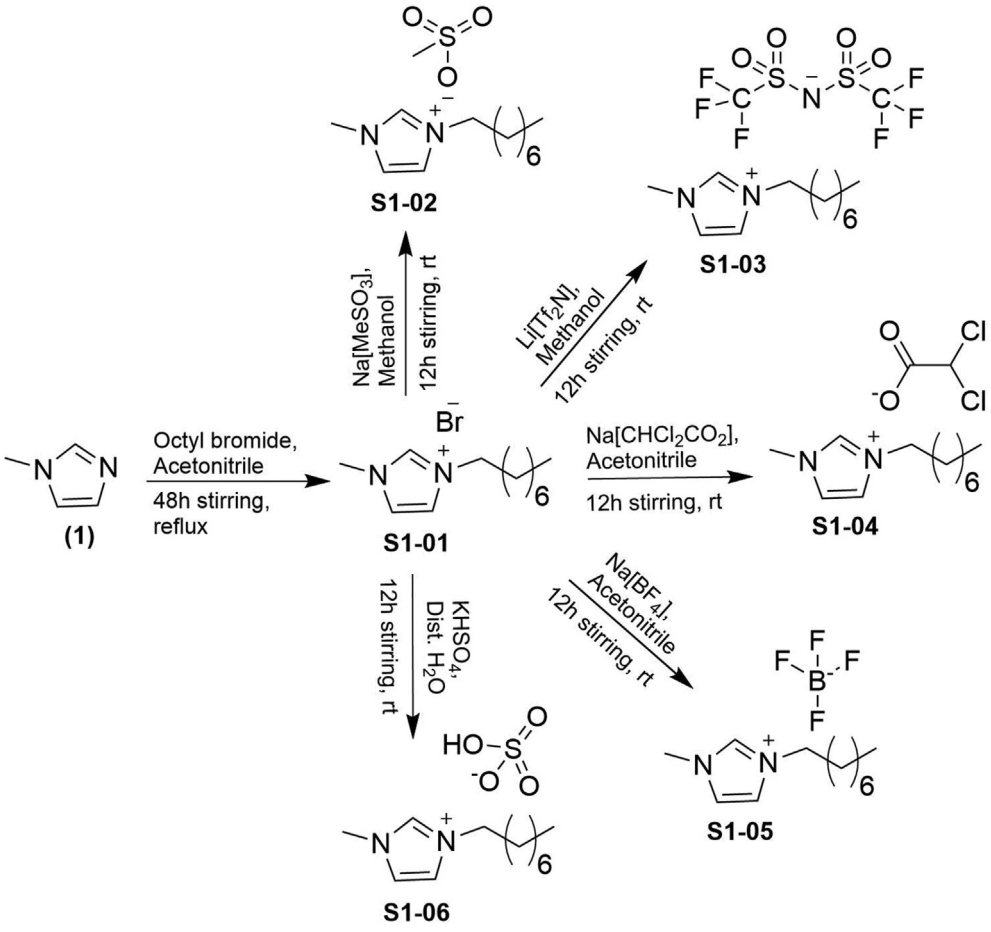


**Scheme 1.** Synthesis of imidazolium-based ILs.

bis(trifluoromethane-sulfonyl) imide (MERCK, 99%), sodium tetrafluoroborate (Sigma-Aldrich, 98%) and sodium hydroxide (Sigma-Aldrich, >98%). Solvents like methanol ($CH_3OH$), chloroform ($CHCl_3$), acetonitrile ($CH_3CN$), n-hexane, and ethyl acetate were dried by distillation before use. The FTIR analysis was performed on the Brucker ATR-alpha FTIR instrument in 4000–550 $cm^{-1}$ to identify the functional groups present in synthesized ionic liquids. The NMR analysis was performed on Brucker NMR (400 MHz) using $CDCl_3$ as a solvent.

### 2.2. Synthesis

#### 2.2.1. Octyl imidazolium based ionic liquids

*2.2.1.1. 1-Methyl-3-octylimidazolium bromide [$C_8$mim][Br].* The [$C_8$mim][Br] was synthesized according to the literature [42]. Briefly, 1-Methylimidazole (5 g, 60 mmol) and octyl bromide (11.74 g, 61 mmol) were added to 60 mL acetonitrile (Scheme 1). The reaction mixture was refluxed for 48 h. After 48 h, the solvent was evaporated by a rotary evaporator. The solid product obtained was dried in a vacuum oven at 50 °C for 12 h. Product (S1-01) was obtained as yellow oily liquid with ~81% yield.

**FTIR ($cm^{-1}$):** 3120 (CH str aromatic), 2924 and 2854 (aliphatic CH str.), 1650 (C=N str.), 1569 (C=C str.), 1463 (CH bending), (1165 C–N str.), 752 (octyl CH bending).

**$^1$H-NMR (ppm) ($CDCl_3$):** 0.37–0.47 (m, 3H; $CH_3$), 0.78–0.86 (m, 2H; $CH_2$), 1.44–1.47 (m, 10H; $CH_2$), 3.60–3.70 (m, 3H; $NCH_3$), 3.87–3.90 (m, 2H; $NCH_2$), 7.21–7.22 (s, 1H; CH = CH), 7.360–7.367 (s, 1H; CH = CH), 9.529–9.531 (s, 1H; N–CH–N). **$^{13}$C-NMR:** 13.66 ($CH_2\mathbf{CH_3}$), 19.13 ($\mathbf{CH_2}CH_3$), 31.84 ($\mathbf{CH_2}CH_2CH_3$), 48.84($NCH_3$), 36.31 ($NCH_2CH_2$), 123.86 (NCH), 122.67 (NCH), 136.94 (NCHN).

*2.2.1.2. 1-Methyl-3-octylimidazolium methanesulphonate [$C_8$mim][$MeSO_3$].* 1-Methyl-octylimidazolium methanesulphonate was synthesized by anion metathesis reaction of [$C_8$mim][Br] and sodium methanesulphonate in methanol (Scheme 1). Briefly, [$C_8$mim][Br] (2.75 g, 10 mmol) and sodium methanesulphonate (4 g, 11.76 mmol) were added to 60 mL methanol and kept on stirring for 12 h. The solvent was evaporated with a rotary evaporator. The NaBr formed during the reaction was removed by solvent extraction using chloroform and ethyl acetate. The product (S1-02) was then dried under vacuum at 50 °C. The yield of the product is ~71%.

**FTIR ($cm^{-1}$):** 3120 (CH str. aromatic), 2924 and 2854 (aliphatic CH str.), 1569 (C=C str.), 1463 (CH bending), 1166 (C–N str.), 1040 (S=O str.), 767 (octyl CH bending).

**$^1$H NMR (400 MHz, $CDCl_3$):** 0.96 (m, 3H; $CH_3$), 1.38 (m, 10H; $CH_2$), 1.89 (m, 2H; $CH_2$), 2.75 (s, 3H; $(SO_3)CH_3$), 4.06 (m, 3H; $NCH_3$), 4.29 (m, 2H; $NCH_2$), 7.60 (s, 1H; CH = CH), 7.70 (s, 1H; CH = CH), **$^{13}$C-NMR:** 13.65 ($CH_2\mathbf{CH_3}$), 19.63 ($\mathbf{CH_2}CH_3$), 32.35 ($\mathbf{CH_2}CH_2CH_3$), 36.51 ($CH_3S$), 40.05 ($NCH_3$), 49.80 ($NCH_2CH_2$), 122.56 (NCH), 124.17 (NCH), 137.88 (NCHN).

*2.2.1.3. 1-Methyl-3-octyl-imidazolium Bis(trifluoromethane-sulfonyl) imide [$C_8$mim][$Tf_2N$].* The [$C_8$mim][Br] (0.3 g, 1 mmol) and lithium bis(trifluoromethane-sulfonyl) imide (0.313 g, 1.1 mmol) were added in two necks round bottom flask containing 60 mL methanol and was evacuated to create an inert atmosphere. The reaction mixture was

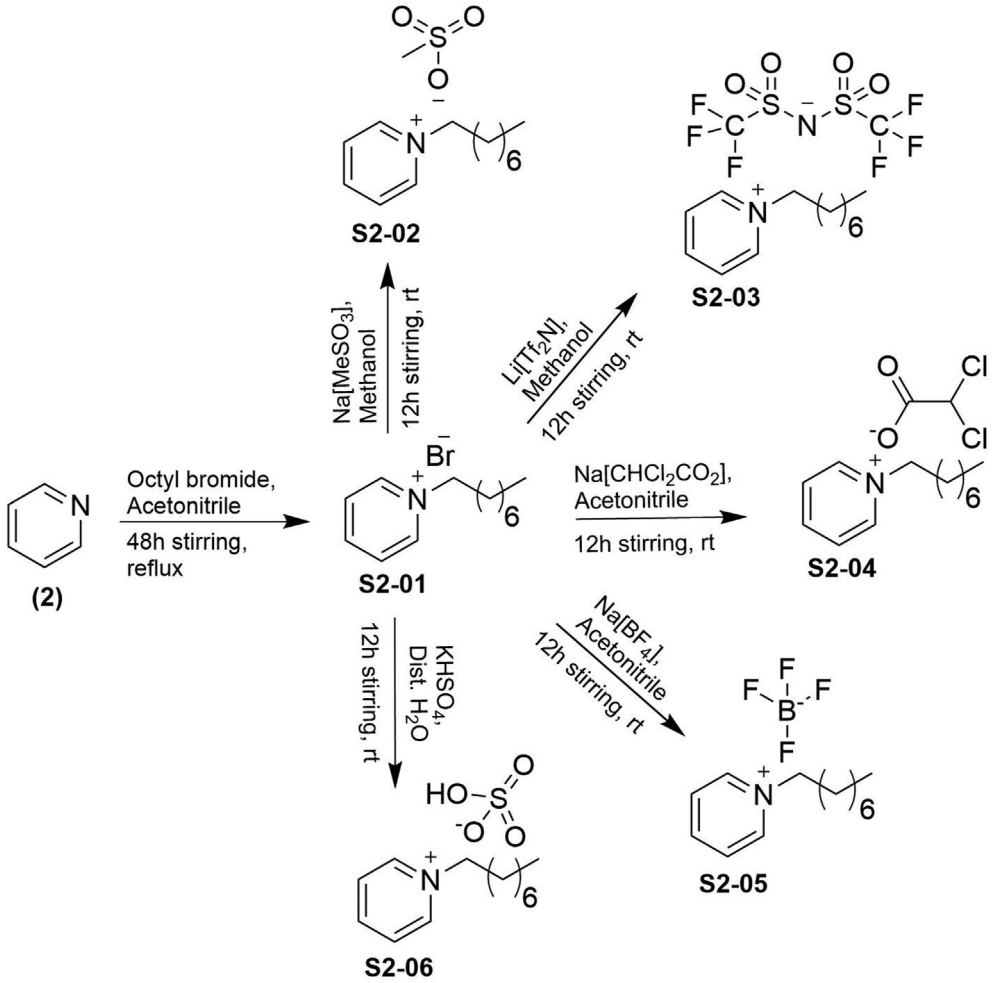


**Scheme 2.** Synthesis of pyridinium-based ILs.

stirred at room temperature for 12 h (Scheme 1). The LiBr formed during the metathesis reaction was removed by solvent extraction followed by filtration. The solvent was evaporated to obtain the pure product (S1-03) and dried overnight under a vacuum at 40 °C. The yield of obtained product is ~75%.

**FTIR ($cm^{-1}$):** 3120 (CH str. aromatic), 2929 and 2854 (aliphatic CH str.), 1569 (C=C str.), 1463 (CH bending), 1358 (S=O asymmetric str.), 1180 (S=O symmetric str.), 1166 (C–N str.), and 739 (octyl CH bending).

**$^1$H NMR (400 MHz, $CDCl_3$):** 0.856–0.822 (m, 3H; CH3), 1.281–1.218 (m, 10H; $CH_2$), 1.836 (m, 2H; CH2), 3.971–3.954 (m, 3H; NCH3), 4.173–4.136 (m, 2H; NCH2), 7.266 (s, 1H; CH = CH), 7.330 (s, 1H; CH = CH), 9.157 (s, 1H; N–CH–N). **$^{13}$C-NMR:** 13.65 ($CH_2$**$CH_3$**), 19.63 (**$CH_2$**$CH_3$), 32.35 (**$CH_2$**$CH_2CH_3$), 36.51 ($CH_3$S), 40.05 ($NCH_3$), 49.80 ($NCH_2CH_2$), 122.56 (NCH), 124.17 (NCH), 137.88 (NCHN).

*2.2.1.4. 1-Methyl-3-octylimidazolium dichloroacetate [$C_8$mim][$CHCl_2CO_2$].* The [$C_8$mim][Br] (0.5 g, 12 mmol) was added to 60 mL acetonitrile and mixed with sodium dichloroacetate (0.3 g, 2 mmol), followed by overnight stirring at room temperature (Scheme 1). The NaBr formed was removed by solvent extraction followed by filtration. The solvent was evaporated to obtain the pure product (S1-04) with a 96% yield.

**FTIR ($cm^{-1}$):** 3120 (CH str. aromatic), 2929 and 2854 (aliphatic CH str.), 1644 (C=O str.), 1571 (C=C str.), 1463 (CH bending), 1358 (C–O str.), 1165 (C–N str.), 740 (Octyl CH bending).

**$^1$H NMR (400 MHz, $CDCl_3$)**: 0.94 (m, 3H; $CH_3$), 1.37 (m, 10H; $CH_2$), 1.552 (1H, s $CHCl_2COO$), 1.92 (m, 2H; $CH_2$), 4.37 (m, 3H; $NCH_3$), 4.07 (m, 2H; $NCH_2$), 7.78 (s, 1H; CH = CH), 7.84 (s, 1H; CH = CH), 9.88 (s, 1H; N–CH–N). **$^{13}$C-NMR:** 13.66 ($CH_2$**$CH_3$**), 19.13 (**$CH_2$**$CH_3$), 31.84 (**$CH_2$**$CH_2CH_3$), 48.84 ($NCH_3$), 36.31 ($NCH_2CH_2$), 67 (**C**$HCl_2COO$) 123.86 (NCH), 122.67 (NCH), 136.94 (NCHN), 167 ($CHCl_2$**C**OO).

*2.2.1.5. 1-Methyl-3-octylimidazolium tetrafluoroborate [$C_8$mim][$BF_4$].* The [$C_8$mim][Br] (0.75 g, 2.72 mmol) solution was slowly added into solution of $NaBF_4$ (0.3 g, 2.7 mmol) in 60 mL acetonitrile. The reaction mixture was stirred overnight under an inert atmosphere at room temperature (Scheme 1). The NaBr formed was separated through filtration and solvent extraction. The solvent was evaporated with a rotary evaporator and dried under a vacuum to obtain the pure product (S1-05) with a 70% yield.

**FTIR ($cm^{-1}$):** 3120 (CH str. aromatic), 2924 and 2854 (aliphatic CH str.), 1569 (C=C str.), 1463 (CH bending), 1165 (C–N str.), 1049 ($BF_4$ anion), 752 (octyl CH bending).

**$^1$H NMR (400 MHz, $CDCl_3$):** 0.86 (m, 3H; $CH_3$), 1.28 (m, 10H; $CH_2$), 1.87 (m, 2H; $CH_2$), 3.94 (m, 3H; $NCH_3$), 4.17 (m, 2H; $NCH_2$), 7.36 (s, 1H; CH = CH), 7.42 (s, 1H; CH = CH), 8.75 (s, 1H; N–CH–N). **$^{13}$C-NMR:** 13.65 ($CH_2$**$CH_3$**), 19.63 (**$CH_2$**$CH_3$), 32.35 (**$CH_2$**$CH_2CH_3$), 40.05 ($NCH_3$), 49.80 ($NCH_2CH_2$), 122.56 (NCH), 124.17 (NCH), 137.88 (NCHN).

*2.2.1.6. 1-Methyl-3-octylimidazolium hydrogen sulfate [$C_8$mim][$HSO_4$].* The [$C_8$mim][Br] (0.5 g, 1.8 mmol) solution was added slowly into the solution of potassium hydrogen sulfate (0.25 g, 1.8 mmol) in distilled water and stirred overnight at room temperature to obtain the product (S1-06) (Scheme 1). The solvent was rotary evaporated, and the

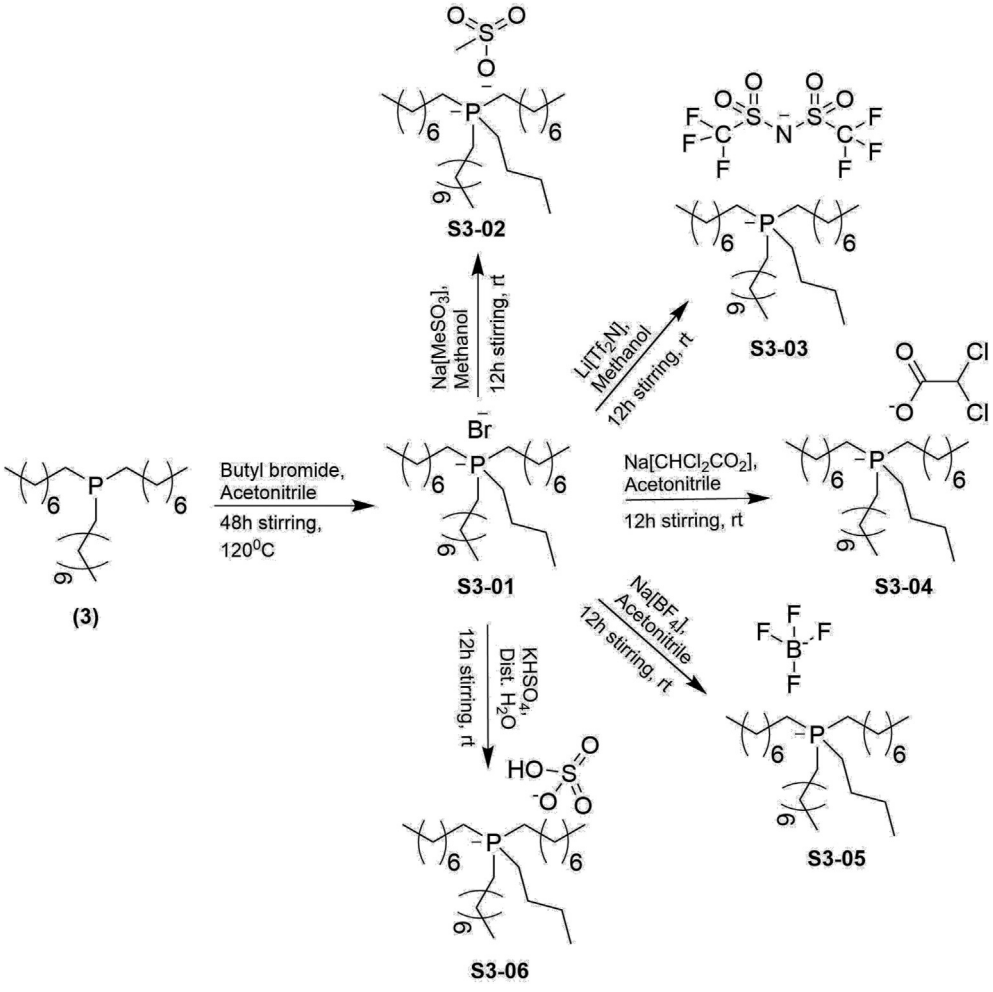


**Scheme 3.** Synthesis of phosphonium-based ILs.

KBr formed was separated through solvent extraction followed by filtration. The product was dried under a vacuum. The yield was 73%.

**FTIR ($cm^{-1}$):** 3120 (CH str. aromatic), 2958 and 2854 (aliphatic CH str.), 1567 (C=C str.), 1463 (CH bending), 1165 (C–N str.), 1047 (S=O str.), 752 (octyl CH bending).

**$^1$H NMR (400 MHz, $CDCl_3$)**: 0.74 (m, 3H; $CH_3$), 1.12 (m, 10H; $CH_2$), 1.68 (m, 2H; $CH_2$), 1.87 (s, 1H; $(SO_4)$H), 2.48 (m, 3H; $NCH_3$), 4.13 (m, 2H; $NCH_2$), 7.57 (s, 1H; CH = CH), 7.71 (s, 1H; CH = CH), 9.06 (s, 1H; N–CH–N). **$^{13}$C-NMR:** 13.65 ($CH_2$**$CH_3$**), 19.63 (**$CH_2$**$CH_3$), 32.35 (**$CH_2$**$CH_2CH_3$), 40.05($NCH_3$), 49.80 ($NCH_2CH_2$), 122.56 (NCH), 124.17 (NCH), 137.88 (NCHN).

### 2.2.2. Octyl pyridinium based ionic liquids

*2.2.2.1. Octyl pyridinium bromide [$C_8$py][Br].* The pyridine (5 g, 63 mmol) and octyl bromide (12.28 g, 63.2mmol) were added to 60 mL acetonitrile and refluxed for 48 h. After 48 h, the solvent was evaporated through the rotary evaporator to obtain the brown-colored crystalline product **(S2-01).** The product was dried in a vacuum oven at 50 °C for 12 h. The product obtained in 95% yield.

**FTIR ($cm^{-1}$):** 3120 (CH str. aromatic), 2924 and 2855 (aliphatic CH str.), 1633 (C=N str.), 1569 (C=C str.), 1486 (CH bending), 1172 (C–N str.), 774 (octyl CH bending).

**$^1$H NMR (400 MHz, $CDCl_3$):** 0.85–0.91 (m, $CH_3$), 1.28–1.32 (m, 10H; $CH_2$), 1.90–1.99 (m, 2H; $CH_2$), 4.88–4.99 (m, 2H; $NCH_2$), 8.10–8.20 (m, 1H; CH pyr-m), 8.55–8.65 (m, 1H; CH pyr-p), 9.45–9.55 (m, 1H; CH pyr-o). **$^{13}$C-NMR:** 13.66 ($CH_2$**$CH_3$**), 19.13 (**$CH_2$**$CH_3$), 31.84 (**$CH_2$**$CH_2CH_3$), 36.31 ($NCH_2CH_2$), 128.82 (CH pyr-m), 144.70 (CH pyr-p), 146.35 (CH pyr-o).

*2.2.2.2. Octyl pyridinium methanesulphonate [$C_8$py][$MeSO_3$].* The 40 mL solution of [$C_8$py][Br] (0.57 g, 2 mmol) in methanol was slowly added to a 40 mL solution of sodium methanesulphonate (0.25 g, 2.1 mmol) and stirred overnight at room temperature to obtain the product (S2-03) (Scheme 2). The NaBr formed was removed by solvent extraction followed by filtration. The solvent was evaporated by a rotary evaporator followed by drying under a vacuum. The yield was 73%.

**FTIR ($cm^{-1}$):** 3120 (CH str. aromatic), 2924 and 2855 (aliphatic CH str.), 1633 (C=N str.), 1569 (C=C str.), 1487 (CH bending), 1174 (C–N str.), 1042 (S=O str.), 774 (octyl CH bending).

**$^1$H NMR (400 MHz, $CDCl_3$):** 0.85–0.91 (m, 3H; oct-$CH_3$), 1.28–1.32 (m, 10H; $CH_2$), 1.90–1.99 (m, 2H; $CH_2$), 2.41 (s, 3H; $CH_3SO_3$), 4.88–4.99 (m, 2H; $NCH_2$), 8.10–8.20 (m, 1H; CH pyr-p), 8.55–8.65 (m, 1H; CH pyr-m), 9.45–9.55 (m, 1H; CH pyr-o). **$^{13}$C-NMR:** 13.66 ($CH_2$**$CH_3$**), 19.63 (**$CH_2$**$CH_3$), 32.84 (**$CH_2$**$CH_2CH_3$), 36.31 ($NCH_2CH_2$), 36.51 ($CH_3$S), 128.82 (CH pyr-m), 144.70 (CH pyr-p), 146.35 (CH pyr-o).

*2.2.2.3. Octyl pyridinium Bis(trifluoromethane-sulfonyl)imide [$C_8$py][$Tf_2N$].* The 30 mL solution of [$C_8$py][Br] (0.3 g, 1.1 mmol) in methanol was slowly added into evacuated 30 mL Li [$Tf_2N$] (0.311 g 1.1 mmol) solution in methanol, followed by overnight stirring under an inert atmosphere (Scheme 2). The LiBr formed was removed by solvent extraction followed by filtration. The remaining solvents were evaporated by a rotary evaporator to obtain the pure product (S2-03). The product was dried overnight in a vacuum oven at 40 °C. The yield was 75%.

**FTIR ($cm^{-1}$):** 3120 (CH str. aromatic), 2924 and 2855 (aliphatic CH str.), 1633 (C=N str.), 1569 (C=C str.), 1345 and 1052 (S=O symmetric and asymmetric str.), 1172 (C–N str.), 774 (octyl CH str.).

**$^1$H NMR (400 MHz, $CDCl_3$):** 0.863–0.817 (m, 3H; oct-CH3), 1.448–1.227 (m, 10H; $CH_2$), 1.964–1.86 (m, 2H; CH2), 2.940 (s, 3H; $CH_3$–C pyr-m), 4.905–4.853 (m, 2H; N–CH2), 7.886–7.860 (m, 1H; CH pyr-m), 7.984–7.939 (m, 1H; CH pyr-p), 8.365–8.313 (m, 1H CH pyr-m), 9.652–9.632 (m, 1H; CH pyr-o). **$^{13}$C-NMR:** 13.66 ($CH_2$**$CH_3$**), 19.63 (**$CH_2$**$CH_3$), 32.84 (**$CH_2$**$CH_2CH_3$), 36.31 ($NCH_2CH_2$), 36.51 ($CH_3$S), 128.82 (CH pyr-m), 144.70 (CH pyr-p), 146.35 (CH pyr-o).

*2.2.2.4. Octyl pyridinium dichloroacetate [$C_8$py][$CHCl_2CO_2$].* The solution of [$C_8$py][Br] (0.54 g, 1.9 mmol) was slowly added to a solution of sodium dichloroacetate (0.3 g, 2 mmol) in 60 mL acetonitrile followed by overnight stirring at room temperature (Scheme 2). The NaBr formed was separated by solvent extraction followed by filtration. The product (S2-04) formed is dried overnight in a vacuum oven. The yield was 90%.

**FTIR ($cm^{-1}$):** 3120 (CH str. aromatic), 2925 and 2855 (aliphatic CH str.), 1633 (C=N str.), 1569 (C=C str.), 1486 (CH bending), 1368 (C–O), 1172 (C–N str.), 772 (octyl CH bending).

**$^1$H NMR (400 MHz, $CDCl_3$)**: 0.94 (m, 3H; $CH_3$), 1.37 (m, 10H; $CH_2$), 1.552 (s, 1H; $CHCl_2COO$), 1.92 (m, 2H; $CH_2$), 7.863 (t, 1H; $NCH_2$), 8.903 (m, 1H; CH pyr-m), 8.991 (m, 1H; CH pyr-p), 9.074 (m, 1H; CH pyr-o). **$^{13}$C-NMR:** 13.66 ($CH_2$**$CH_3$**), 19.13 (**$CH_2$**$CH_3$), 31.84 (**$CH_2$**$CH_2CH_3$), 36.31 ($NCH_2CH_2$), 67 (**C**$HCl_2COO$), 128.82 (CH pyr-m), 144.70 (CH pyr-p), 146.35 (CH pyr-o), 167($CHCl_2$**C**OO).

*2.2.2.5. Octyl pyridinium tetrafluoroborate [$C_8$py][$BF_4$].* The 30 mL solution of [$C_8$py][Br] (0.7 g, 2.5 mmol) was added into evacuated 30 mL solution of sodium tetrafluoroborate (0.3 g, 2.7 mmol) followed by overnight stirring under nitrogen atmosphere at room temperature (Scheme 2). The NaBr formed was separated by solvent extraction followed by filtration. The solvent was evaporated to obtain the product (S2-05) and dried overnight in a vacuum oven. The yield was 70%.

**FTIR ($cm^{-1}$):** 3120 (CH str. aromatic), 2926 and 2855 (aliphatic CH str.), 1633 (C=N str.), 1569 (C=C str.), 1489 (CH bending), 1172 (C–N str.), 1033 ($BF_4$ anion), 774 (octyl CH bending).

**$^1$H NMR (400 MHz, $CDCl_3$):** 0.804–0.770 (m, 3H; oct-$CH_3$), 1.260–1.166 (m, 10H; $CH_2$), 1.927–1.891 (m, 2H; CH2), 2.596 (s, 3H; CH3 pyr-p), 4.511–4.473 (m, 2H; N–$CH_2$), 7.794–7.778 (m, 1H; CH pyr-m), 8.658–8.641 (2H, m, CHpyr-o). **$^{13}$C-NMR:** 13.66 ($CH_2$**$CH_3$**), 19.63 (**$CH_2$**$CH_3$), 32.84 (**$CH_2$**$CH_2CH_3$), 36.31 ($NCH_2CH_2$), 128.82 (CH pyr-m), 144.70 (CH pyr-p), 146.35 (CH pyr-o).

*2.2.2.6. Octyl pyridinium hydrogen sulfate [$C_8$py][$HSO_4$].* The solution of [$C_8$py][Br] (0.6g, 2.3 mmol) was slowly added to the solution of potassium hydrogen sulfate (0.3g, 2.2 mmol) and stirred overnight at room temperature (Scheme 2). The KBr formed during the anion metathesis reaction was separated by solvent extraction followed by filtration. The solvent was evaporated by a rotary evaporator, and the product was vacuum dried to obtain the product (S2-06) with ~75% yield.

**FTIR ($cm^{-1}$):** 3120 (CH str. aromatic), 2923 and 2854 (aliphatic CH str.), 1632 (C=N str.), 1569 (C=C str.), 1486 (CH bending), 1169 (C–N str.), 1046 (S=O str.), 774 (octyl CH bending).

**$^1$H NMR (400 MHz, $CDCl_3$)**: 0.74 (m, 3H; $CH_3$), 1.12 (m, 10H; $CH_2$), 1.68 (m, 2H; $CH_2$), 1.87 (s, 1H; $(SO_4)$H), 2.48 (m, 3H; $NCH_3$), 4.13 (m, 2H; $NCH_2$), 7.57 (s, 1H; CH = CH), 7.71 (s, 1H; CH = CH), 9.06 (s, 1H; N–CH–N). **$^{13}$C-NMR:** 13.66 ($CH_2$**$CH_3$**), 19.63 (**$CH_2$**$CH_3$), 32.84 (**$CH_2$**$CH_2CH_3$), 36.31 ($NCH_2CH_2$), 128.82 (CH pyr-m), 144.70 (CH pyr-p), 146.35 (CH pyr-o).

### 2.2.3. Phosphonium based ionic liquids

*2.2.3.1. Mono-butyl tri-octyl phosphonium bromide [$P_{4888}$][Br].* The trioctyl phosphine (5 g, 13.5 mmol, and 6.02 mL) was mixed with butyl bromide (1.85 g, 13.5 mmol) in a round bottom flask containing acetonitrile and evacuated to create an inert atmosphere and refluxed at 120 °C. When TLC confirmed the completion of the reaction, the solvents

**Table 1.** Antibacterial activity of octyl imidazolium-based ILs.

| ILs | Bacterial Strains | | | | | | |
|---|---|---|---|---|---|---|---|
| | *E. coli* | *E. aerogenes* | *K. pneumoniae* | *P. vulgaris* | *P. aeruginosa* | *S. pneumoniae* | *S. pyogenes* |
| **- control** | 0 | 0 | 0 | 0 | 0 | 0 | 0 |
| **+ control** | 17 | 27 | 12 | 25 | 27 | 25 | 30 |
| **S1-01** | 21 | 25 | 19 | 20 | 25 | 22 | 14 |
| **S1-02** | 21 | 27 | 20 | 18 | 24 | 17 | 13 |
| **S1-03** | 15 | 17 | 17 | 10 | 17 | 20 | 20 |
| **S1-04** | 19 | 17 | 16 | 17 | 20 | 23 | 15 |
| **S1-05** | 18 | 22 | 15 | 19 | 15 | 17 | 20 |
| **S1-06** | 12 | 17 | 17 | 17 | 11 | 0 | 20 |

were removed by evaporation to obtain the product (S3-01) as a dark yellow oily liquid. It was dried in a vacuum oven at 50 °C for 12 h. The yield was 91%.

**FTIR ($cm^{-1}$):** 2960 and 2854 (CH str.), 1463 (CH bending), 746 (octyl and butyl CH bending).

**$^1$H NMR (400 MHz, $CDCl_3$):** 0.913–0.942 (t, 3H; $CH_2\mathbf{CH_3}$), 1.395–1.499 (m, 2H; $\mathbf{CH_2}CH_3$), 2.152–2.211 (m, 2H; $\mathbf{CH_2}CH_2CH_3$), 2.508–2.515 (t, 2H; $\mathbf{P–CH_2}$). **$^{13}$C-NMR:** 13.685 ($CH_2\mathbf{CH_3}$), 17.633 ($\mathbf{CH_2}CH_3$), 23.093 ($\mathbf{CH_2}CH_2CH_3$), 23.761 (**P– $\mathbf{CH_2}$**).

*2.2.3.2. Mono-butyl tri-octyl phosphonium methanesulphonate [$P_{4888}$][$MeSO_3$].* The solution of [$P_{4888}$][Br] (1 g, 1.9 mmol) in 40 mL methanol was slowly added to the solution of sodium methanesulphonate (0.23 g, 1.9 mmol) in 40 mL methanol, followed by overnight stirring at room temperature to obtain the product (S3-02) (Scheme 3). After the completion of the reaction, the NaBr formed was removed by solvent extraction, and unreacted methanol was removed by evaporation. The product was then dried in a vacuum oven. The yield was 73%.

**FTIR ($cm^{-1}$):** 2920 and 2854 (CH str.), 1461 (CH bending), 1236 and 1161 (symmetric and asymmetric CH str.), 749 (octyl and butyl CH bending).

**$^1$H NMR (400 MHz, $CDCl_3$):** 0.913–0.942 (t, 3H; $CH_2\mathbf{CH_3}$), 1.395–1.499 (m, 2H; $\mathbf{CH_2}CH_3$), 2.152–2.211 (m, 2H; $\mathbf{CH_2}CH_2CH_3$), 2.508–2.515 (t, 2H; $\mathbf{P–CH_2}$). **$^{13}$C-NMR:** 13.685 ($CH_2\mathbf{CH_3}$), 17.633 ($\mathbf{CH_2}CH_3$), 23.093 ($\mathbf{CH_2}CH_2CH_3$), 23.761 (**P–$\mathbf{CH_2}$**), 36.51 ($CH_3S$).

*2.2.3.3. Mono-butyl tri-octyl phosphonium Bis(trifluoromethane-sulfonyl) imide [$P_{4888}$][$Tf_2N$].* The [$P_{4888}$][Br] (1.0 g, 1.9 mmol) was dissolved in 30 mL methanol to form a solution. The Bis(trifluoromethane-sulfonyl) imide (0.5 g, 1.8 mmol) was added in two necks round bottom flask containing 30 mL methanol. Air in the flask was removed to create an inert atmosphere. The solution of [$P_{4888}$][Br] was added to the evacuated flask, followed by overnight stirring under a nitrogen atmosphere at room temperature (Scheme 3). The LiBr formed was separated by solvent extraction followed by filtration. The rotary evaporator removed the excess solvent to obtain the product (S3-03) and further dried overnight in a vacuum oven at 40 °C. The yield was 83%.

**FTIR ($cm^{-1}$):** 2929 and 2854 (CH str.), 1463 (CH bending), 1347 and 1056 (S=O str.), 746 (octyl and butyl CH bending).

**$^1$H NMR (400 MHz, $CDCl_3$):** 0.913–0.942 (t, 3H; $CH_2\mathbf{CH_3}$), 1.395–1.499 (m, 2H; $\mathbf{CH_2}CH_3$), 2.152–2.211 (m, 2H; $\mathbf{CH_2}CH_2CH_3$), 2.508–2.515 (t, 2H; $\mathbf{P–CH_2}$). **$^{13}$C-NMR:** 13.685 ($CH_2\mathbf{CH_3}$), 17.633 ($\mathbf{CH_2}CH_3$), 23.093 ($\mathbf{CH_2}CH_2CH_3$), 23.761 (**P–$\mathbf{CH_2}$**), 36.51 ($CH_3S$).

*2.2.3.4. Mono-butyl tri-octyl phosphonium dichloroacetate [$P_{4888}$][$CHCl_2CO_2$].* The sodium dichloroacetate (0.3 g, 2 mmol) solution was added into an evacuated solution of [$P_{4888}$][Br] (1 g, 1.9 mmol) in 80 mL acetonitrile which was followed by overnight stirring under an inert atmosphere at room temperature (Scheme 3). The NaBr formed was filtered, and the solvent was evaporated. Pure product (S3-04) was obtained by solvent extraction and filtration followed by overnight drying in a vacuum oven. The yield was 85%.

**FTIR ($cm^{-1}$):** 2923 and 2854 (CH str.), 1463 (CH bending), 1651 (C=O str.), 1376 (C–O str.), 711 (octyl and butyl CH bending).

**$^1$H NMR (400 MHz, $CDCl_3$):** 0.913–0.942 (t, 3H; $CH_2\mathbf{CH_3}$), 1.395–1.499 (m, 2H; $\mathbf{CH_2}CH_3$), 2.152–2.211 (m, 2H; $\mathbf{CH_2}CH_2CH_3$), 2.508–2.515 (t, 2H; $\mathbf{P–CH_2}$). **$^{13}$C-NMR:** 13.685 ($CH_2\mathbf{CH_3}$), 17.633 ($\mathbf{CH_2}CH_3$), 23.093 ($\mathbf{CH_2}CH_2CH_3$), 23.761 (**P–$\mathbf{CH_2}$**), 67 ($CHCl_2COO$), 167($CHCl_2\mathbf{C}OO$).

*2.2.3.5. Mono-butyl tri-octyl phosphonium tetrafluoroborate [$P_{4888}$][$BF_4$].* The [$P_{4888}$][Br] (1 g, 1.9 mmol) was dissolved in 30 mL acetonitrile to form a solution. The sodium tetrafluoroborate (0.2 g, 1.8 mmol) was also dissolved in 30 mL acetonitrile in a round bottom flask and evacuated to remove excess air. The [$P_{4888}$][Br] solution was added to evacuated sodium tetrafluoroborate solution, followed by overnight stirring under a nitrogen atmosphere at room temperature (Scheme 3). The NaBr formed was separated by filtration, and excess solvent was evaporated. The product (S3-05) was obtained by overnight drying in a vacuum oven. The yield was 70%.

**FTIR ($cm^{-1}$):** 2924 and 2855 (CH str.), 1463 (CH bending), 1049 ($BF_4$ ion), 751 (octyl and butyl CH bending).

**$^1$H NMR (400 MHz, $CDCl_3$):** 0.913–0.942 (t, 3H; $CH_2\mathbf{CH_3}$), 1.395–1.499 (m, 2H; $\mathbf{CH_2}CH_3$), 2.152–2.211 (m, 2H; $\mathbf{CH_2}CH_2CH_3$), 2.508–2.515 (t, 2H; $\mathbf{P–CH_2}$). **$^{13}$C-NMR:** 13.685 ($CH_2\mathbf{CH_3}$), 17.633 ($\mathbf{CH_2}CH_3$), 23.093 ($\mathbf{CH_2}CH_2CH_3$), 23.761 (**P–$\mathbf{CH_2}$**).

*2.2.3.6. Mono-butyl tri-octyl phosphonium hydrogen sulfate [$P_{4888}$][$HSO_4$].* The [$P_{4888}$][Br] (1 g, 1.9 mmol) was dissolved in 30 mL distilled water to form solution A. The potassium hydrogen sulfate (0.2 g, 1.4 mmol) was dissolved in 30 mL of distilled water to obtain solution B. Both solutions A and B, were mixed and kept on stirring for 12 h (Scheme 3). The KBr formed was removed by solvent extraction using chloroform followed by filtration. The pure product (S3-06) is obtained by overnight drying in a vacuum oven. The yield was 71%.

**FTIR ($cm^{-1}$):** 2923 and 2854 (CH str.), 1460 (CH bending), 1236 and 1161 (S=O str.), 719 (octyl and butyl CH str.).

**$^1$H NMR (400 MHz, $CDCl_3$):** 0.913–0.942 (t, 3H; $CH_2\mathbf{CH_3}$), 1.395–1.499 (m, 2H; $\mathbf{CH_2}CH_3$), 2.152–2.211 (m, 2H; $\mathbf{CH_2}CH_2CH_3$), 2.508–2.515 (t, 2H; $\mathbf{P–CH_2}$). **$^{13}$C-NMR:** 13.685 ($CH_2\mathbf{CH_3}$), 17.633 ($\mathbf{CH_2}CH_3$), 23.093 ($\mathbf{CH_2}CH_2CH_3$), 23.761 (**P–$\mathbf{CH_2}$**).

### 2.3. Antibacterial activity

The samples of equal density and potency were prepared using distilled water. Each sample was tested in triplicate. Eighteen samples were used to check their antibacterial activity against pathogenic bacteria. New bacterial culture of 24 h was used to make the lawn in Petri dishes. About 100 μl of each equalized bacterial sample was spread on Petri dishes. Using a sterilized borer, 3 mm wells were made at equal

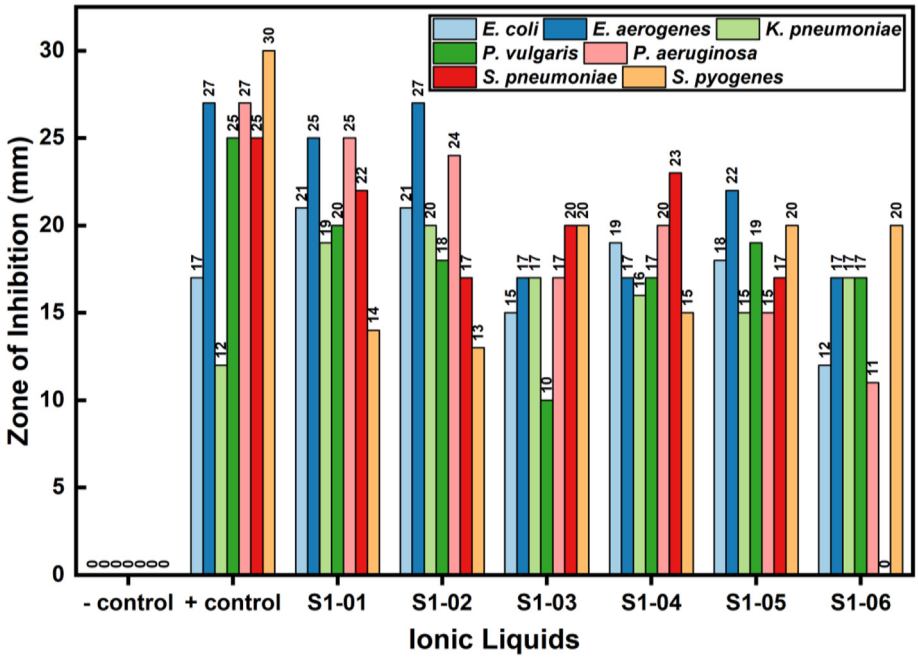


**Figure 1.** Antibacterial activity of imidazolium-based ILs.

distances. Positive and negative controls were used in equal v/v ratio on every plate. About 25 μl of sample solutions were poured into each well and then incubated for 24 h at 37 °C. The distilled water was used as negative control and levofloxacin as the positive control [43].

### 2.4. Computational studies

#### 2.4.1. Density functional theory studies

All the ILs were modeled, and their geometry optimizations were performed at the B3LYP/6-31g level of Density Functional Theory methods [44] using the Gaussian 09 program. The geometry optimization was performed in the vacuum keeping the overall charge zero for all the ILs. For validation purposes, frequency calculations were performed on the optimized geometries using the same level of the DFT method used for optimization. As the application of these ILs was to act as inhibitors for the protein, single-point energy on all the optimized geometries was calculated in the aqueous medium with the same method and basis set enhanced by polarization functions for all atoms except hydrogen.

#### 2.4.2. Molecular docking studies

Molecular docking was performed to understand the binding affinity between the target protein, β-lactamase, and the designed ILs [45, 46, 47, 48]. As the β-lactamase enzymes are involved in the antibiotic resistance by hydrolyzing the peptide bond of the β-lactam ring, therefore the

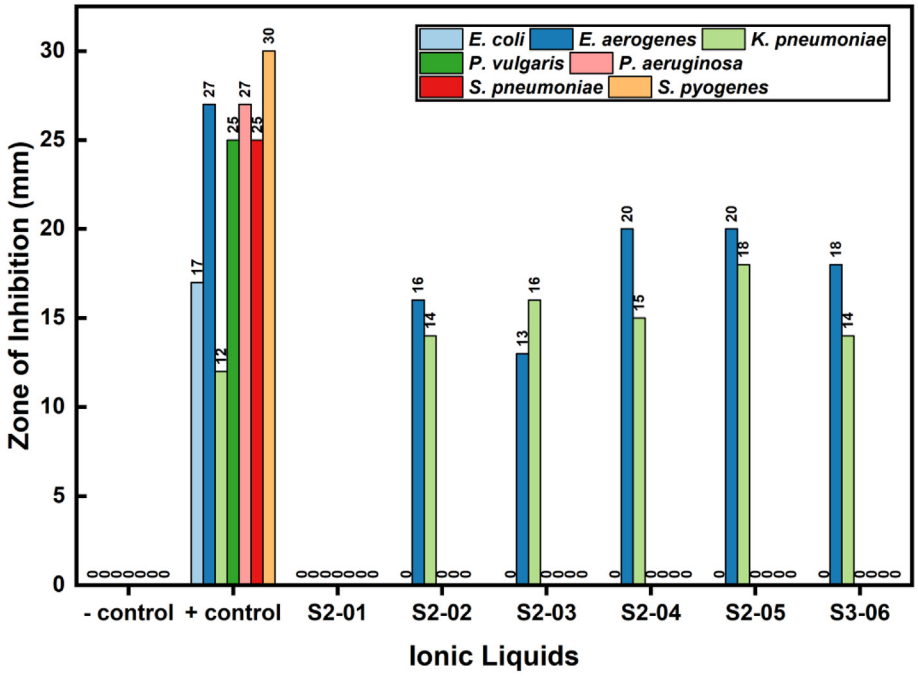


**Figure 2.** Antibacterial activity of pyridinium-based ILs.

**Table 2.** Anti-bacterial activity of octyl pyridinium-based ILs.

| ILs | Bacterial Strains | |
|---|---|---|
| | *E. aerogenes* | *K. pneumoniae* |
| **S2-01** | 0 | 0 |
| **S2-02** | 16 | 14 |
| **S2-03** | 13 | 16 |
| **S2-04** | 20 | 15 |
| **S2-05** | 20 | 18 |
| **S2-06** | 18 | 14 |

**Table 3.** Anti-bacterial activities of Phosphonium-based ILs.

| ILs | Bacterial Strains | |
|---|---|---|
| | *E. coli* | *E. aerogenes* |
| **S3-01** | 0 | 9 |
| **S3-02** | 12 | 14 |
| **S3-03** | 9 | 9 |
| **S3-04** | 11 | 13 |
| **S3-05** | 10 | 14 |
| **S3-06** | 10 | 13 |

β-lactamase enzymes of the six gram-positive and gram-negative bacteria; *E. coli* (PDB ID: 5A92) [49] *E. aerogenes* (PDB ID: 5KID) [50], *K. pneumonia* (PDB ID: 6MGX) [51], *P. vulgaris* (PDB ID: 1HZO), *P. aeruginosa* (PDB ID: 4GZB) [52], and *S. pneumoniae* (PDB ID: 1RPS) [53] are used for molecular docking. For docking purposes, optimized geometry of all the ILs geometries was used. Molecular docking studies were performed using PyRx software where the optimized ILs and the proteins (PDB structure) were loaded, and molecular docking was performed after the selection of the predicted protein chains. Before docking, all the protein structure's energy was minimised where protonation and water molecules were removed. Default settings were maintained for all parameters during the docking process. As a result of docking, nine different conformations were generated for every pair of protein and ligand. The conformation with the highest Binding Affinity was selected for evaluation.

## 3. Result and discussion

ILs based on imidazolium, pyridinium, and phosphonium with different anions (bromide, hydrogen sulfate, dichloroacetate, bis(trifluoromethane sulfonyl)imide, tetrafluoroborate, and methanesulphonate, etc.) were prepared and characterized with the help of characterization techniques (TLC, ATR-FTIR, NMR, etc.) at different levels during and after the synthesis.

### 3.1. Imidazolium-based ionic liquids

The Methyl imidazole (1) was reacted with octyl bromide under reflux for 48 h in acetonitrile as a solvent to give **S1-01.** $^{1}$H-NMR confirmed the successful synthesis of S1-01 as the peaks for aromatic proton (NCHN) shifts from 7.385 ppm in (1) to 9.53 ppm in product **S1-01.** The quaternization of (1) is confirmed by shifting the –$CH_2$ peak from 3.35 ppm in octyl bromide to 3.87–3.90 ppm in product **S1-01.** FTIR of **S1-01** indicates quaternarization of methyl imidazole with octyl bromide. The following peaks were observed in FTIR of **S1-01;** 3120 $cm^{-1}$ (aromatic CH stretch), 2924 $cm^{-1}$, and 2854 $cm^{-1}$ (aliphatic CH stretch) for $CH_2$ and $CH_3$, respectively. 1650 $cm^{-1}$ (C=N stretch), 1569 $cm^{-1}$ (C=C stretch), 1463 $cm^{-1}$ ($CH_2$ bend), 1165 $cm^{-1}$ (C–N stretch), 752 $cm^{-1}$ (long-chain $CH_2$ of octyl group).

FTIR indicated the formation of **S1-02** due to band appearance at 1040 $cm^{-1}$ responsible for S=O stretch. This characteristic band appears due to the exchange of anions. The formation of **S1-03** was confirmed by FTIR due to the appearance of peaks at 1358 $cm^{-1}$, indicating asymmetric stretching vibration of S=O and at 1180 $cm^{-1}$ symmetric stretching vibration of S=O. The C=O and C–O stretching bands at 1644 $cm^{-1}$ and 1358 $cm^{-1}$, respectively, indicate the formation of **S1-04.** The formation of **S1-05** was confirmed by the presence strong band at 1049 $cm^{-1}$ due to [$BF_4$] anion. A peek at 1047 $cm^{-1}$ due to S=O shows the formation of **S1-06.**

### 3.2. Pyridinium based ionic liquids

The pyridine (2) was reacted with octyl bromide under reflux for 48 h to give **S2-01** as the product (Scheme 2). $^{1}$H-NMR confirmed the formation of **S2-01** as the peaks for aromatic protons (Pyr-o/Pyr-m/Pyr-p)

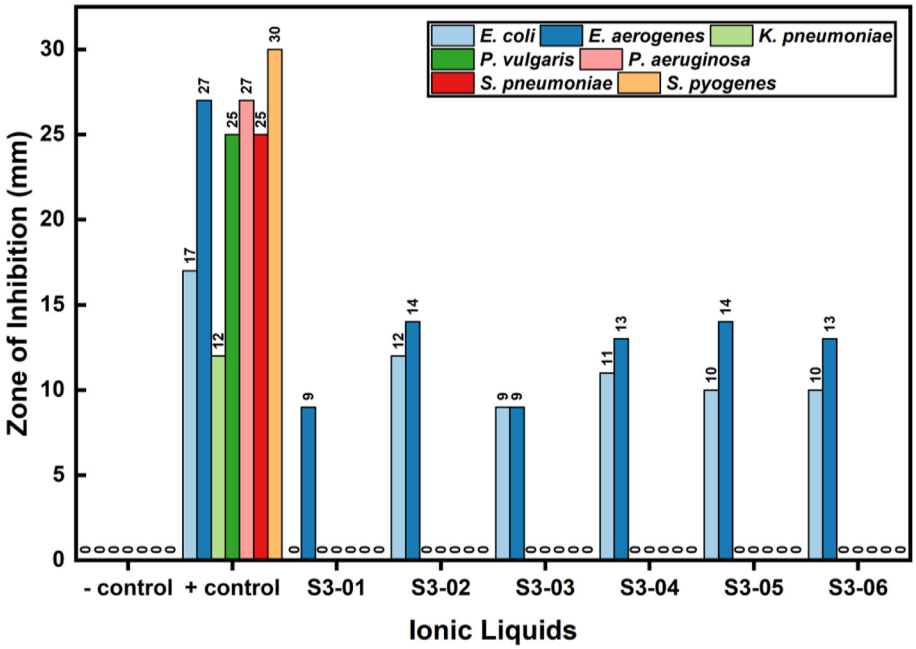


**Figure 3.** Antibacterial activity of phosphonium-based ILs.

**Table 4.** Molecular docking scores of Binding affinity in Kcal/mol (RMSD values).

| IONIC LIQUIDS | | | BACTERIAL STRAINS | | | | | |
|---|---|---|---|---|---|---|---|---|
| Cations | Anions | Label | *E. coli* | *E. aerogenes* | *K. pneumoniae* | *P. vulgaris* | *P. aeruginosa* | *S. pneumoniae* |
| **Imidazolium** | **Br** | **S1-01** | -4 (5.14) | -4.6 (2.08) | -4.5 (34.34) | -4.5 (3.84) | -4.7 (2.54) | -4.3 (45.4) |
| | **[$CH_3SO_3$]** | **S1-02** | -4.9 (4.2) | -5 (4.38) | -5.1 (2.42) | -4.8 (4.47) | -4.8 (7.11) | -5.2 (25.63) |
| | **[$Tf_2N$]** | **S1-03** | **-6.6 (2.06)** | **-7.7 (2.70)** | **-6.3 (3.78)** | **-6.8 (5.73)** | **-7.7 (2.88)** | **-7.7 (5.46)** |
| | **[$CHCl_2CO_2$]** | **S1-04** | -4.9 (2.64) | -5.3 (2.91) | -4.9 (2.58) | -4.7 (6.94) | -5.0 (5.23) | -4.7 (2.99) |
| | **[$BF_4$]** | **S1-05** | -4.8 (3.14) | -3.5 (2.09) | -3.2 (2.09) | -3.2 (2.10) | -3.2 (2.11) | -4.0 (2.09) |
| | **[$HSO_4$ ]** | **S1-06** | -5.5 (6.99) | -5.4 (2.36) | -5.3 (3.81) | -6.4 (2.01) | -6 (6.67) | -6 (4.56) |
| **Pyridinium** | **Br** | **S2-01** | -4.6 (3.28) | -5.0 (2.73) | -4.6 (3.25) | -4.5 (3.48) | -4.9 (6.06) | -5.3 (6.64) |
| | **[$CH_3SO_3$]** | **S2-02** | -4.9 (5.43) | -5.8 (6.49) | -5.2 (3.50) | -4.7 (3.40) | -5.8 (4.76) | -5.7 (5.75) |
| | **[$Tf_2N$]** | **S2-03** | **-7.1 (4.73)** | **-7.3 (3.99)** | **-6.4 (5.25)** | **-6.7 (2.12)** | **-7.5 (2.07)** | **-8.4 (2.23)** |
| | **[$CHCl_2CO_2$]** | **S2-04** | -5.6 (2.73) | -5.7 (2.14) | -5.0 (2.49) | -5.0 (5.56) | -5.3 (6.17) | -6.1 (2.29) |
| | **[$BF_4$]** | **S2-05** | -3.5 (1.84) | -3.5 (2.11) | -3.3 (2.10) | -3.2 (2.26) | -3.2 (1.82) | -3.7 (1.82) |
| | **[$HSO_4$ ]** | **S2-06** | -5.2 (2.31) | -5.6 (4.37) | -5.2 (18.75) | -5.1 (6.39) | -6.1 (6.37) | -6.2 (2.71) |
| **Phosphonium** | **Br** | **S3-01** | -3.9 (7.59) | -4.9 (2.03) | -4.1 (3.76) | -3.9 (5.07) | -4.4 (4.15) | -4.9 (5.41) |
| | **[$CH_3SO_3$]** | **S3-02** | -4.5 (6.40) | -4.8 (2.01) | -4.5 (5.94) | -4.1 (5.41) | -4.5 (3.41) | -5.9 (2.64) |
| | **[$Tf_2N$]** | **S3-03** | **-5.2 (3.75)** | -6 (3.30) | **-4.9 (3.75)** | **-5.1 (8.95)** | **-5.7 (3.45)** | -5.1 (4.81) |
| | **[$CHCl_2CO_2$]** | **S3-04** | -4.5 (31.75) | -4.9 (2.82) | -4.2 (6.173) | -4.6 (7.37) | -4.7 (5.54) | -4.5 (6.26) |
| | **[$BF_4$]** | **S3-05** | -3.5 (2.10) | -3.5 (2.10) | -3.3 (19.09) | -3.2 (2.44) | -3.2 (1.83) | -3.7 (2.60) |
| | **[$HSO_4$ ]** | **S3-06** | -5 (5.40) | **-6.1 (7.29)** | -4.9 (2.032) | -5.1 (3.01) | -5.7 (5.61) | -4.6 (6.87) |

shifts downfield from 8.613/7.277/7.65 ppm in (2) to 9.45–9.55/8.1–8.2/8.55–8.65 ppm in product **S2-01.** The peak due to the –$CH_2$ group of octyl bromide also shifts from 3.35 ppm to 4.88–4.99 ppm after quaternization of (2). FTIR also confirmed the quaternization of (2) with octyl bromide. Following bands are appeared in FTIR of **S2-01**; 3120 $cm^{-1}$ (aromatic CH stretch), 2924 $cm^{-1}$ and 2855 $cm^{-1}$ (aliphatic CH stretch) for $CH_2$ and $CH_3$ respectively, 1633 $cm^{-1}$ (C=N stretch), 1569 $cm^{-1}$ (C=C stretch), 1486 $cm^{-1}$ ($CH_2$ bend), 1172 $cm^{-1}$ (C–N stretch), 774 $cm^{-1}$ (long-chain $CH_2$ of octyl group).

FTIR for **S2-02** shows S=O stretching vibration at 1042 $cm^{-1,}$ indicating the exchange of methane sulphonate anion. In FTIR for **S2-03,** the bands at 1345 $cm^{-1}$ and 1052 $cm^{-1}$ are due to S=O stretching. The C=O and C–O stretching bands appear at 1633 $cm^{-1}$ and 1368$cm^{-1}$, respectively, indicating the formation of **S2-04.** The formation of **S2-05** was confirmed by the presence of a strong band at 1033 $cm^{-1}$ due to [$BF_4$] anion. The peak at 1046 $cm^{-1}$ appears due to S=O stretching, indicating **S2-06** formation.

### 3.3. Phosphonium based ionic liquids

The tri-octyl phosphine (3) was reacted with butyl bromide under an inert atmosphere at 120 °C for 48 h to give **S3-01** as the product. $^1$H-NMR confirmed the quaternization of (3) as the –$CH_2$ peak shifts from 3.35 ppm in butyl bromide to 2.508–2.525 ppm in product **S3-01.** FTIR of **S3-01** also confirms the quaternarization of tri-octyl phosphine with butyl bromide. Following bands appeared in FTIR of **S3-01**; 2960 $cm^{-1}$ and 2854 $cm^{-1}$ (CH stretch), 1463 $cm^{-1}$ ($CH_2$ bend), and 746 $cm^{-1}$ (long-chain $CH_2$ in butyl and octyl groups attached to phosphorous).

The S=O stretching vibration at 1347 $cm^{-1}$ and 1056 $cm^{-1}$ in FTIR of **S3-03** confirms its formation by replacing bromide anion. The C=O and C–O stretching vibration at 1651 $cm^{-1}$ and 1376 $cm^{-1}$, respectively, indicate the formation of **S3-04** by replacing dichloroacetate with bromide anion. The formation of **S3-05** was confirmed by the presence of a band at 1049 $cm^{-1}$ due to [$BF_4$] anion. The S=O stretching vibrations at 1236 $cm^{-1}$ and 1161 $cm^{-1}$ indicate the formation of **S3-06.**

### 3.4. Antibacterial activity

Compared to other living organisms, the short generation time of bacteria had indirectly led the researchers to investigate the antibacterial activity of ILs [54]. The toxicity of pyridinium, phosphonium, and imidazolium-based ILs increases with alkyl chain length in their quaternary ammonium salts [55, 56]. In this study, 18 different ILs were synthesized to check their potential toxicity and effectiveness as antibacterial agents against gram-positive and gram-negative bacterial

**Table 5.** Molecular docking results: important interactions for the high binding affinity models.

| IONIC LIQUIDS | | | BACTERIAL STRAINS | | | | | |
|---|---|---|---|---|---|---|---|---|
| Cations | Anions | Label | *E. coli* | *E. aerogenes* | *K. pneumoniae* | *P. vulgaris* | *P. aeruginosa* | *S. pneumoniae* |
| **Imidazolium** | **[$Tf_2N$]** | **S1-03** | Lys-73 | Met-217, Phe-122 | SerB-217, Gly-B219, Lys-B211 | Thr-216, Asn-132 | Ser-64, Ser-319 | Arg-652, Val-662 |
| **Pyridinium** | **[$Tf_2N$]** | **S2-03** | Ser-237 | Thr-316, Asn-340 | His-A189, His-B189, Asn-A220, Asn-B220, His-A250, His-B250 | Ser-130, Ser-237 | Tyr-151, Asn-347 | Lys-420, Arg-654 |
| **Phosphonium** | **[$CH_3SO_3$]** | **S3-02** | - | - | - | - | - | Gly-664, Pro-697 |
| | **[$Tf_2N$]** | **S3-03** | Ser-130, Ser-237 | - | Lys-211, His-260 | Lys-147 | Ser-319, Asn-344, Asn-347 | - |
| | **[$HSO_4$ ]** | **S3-06** | - | Ser-65, Tyr-151, Ser-315 | - | - | - | - |

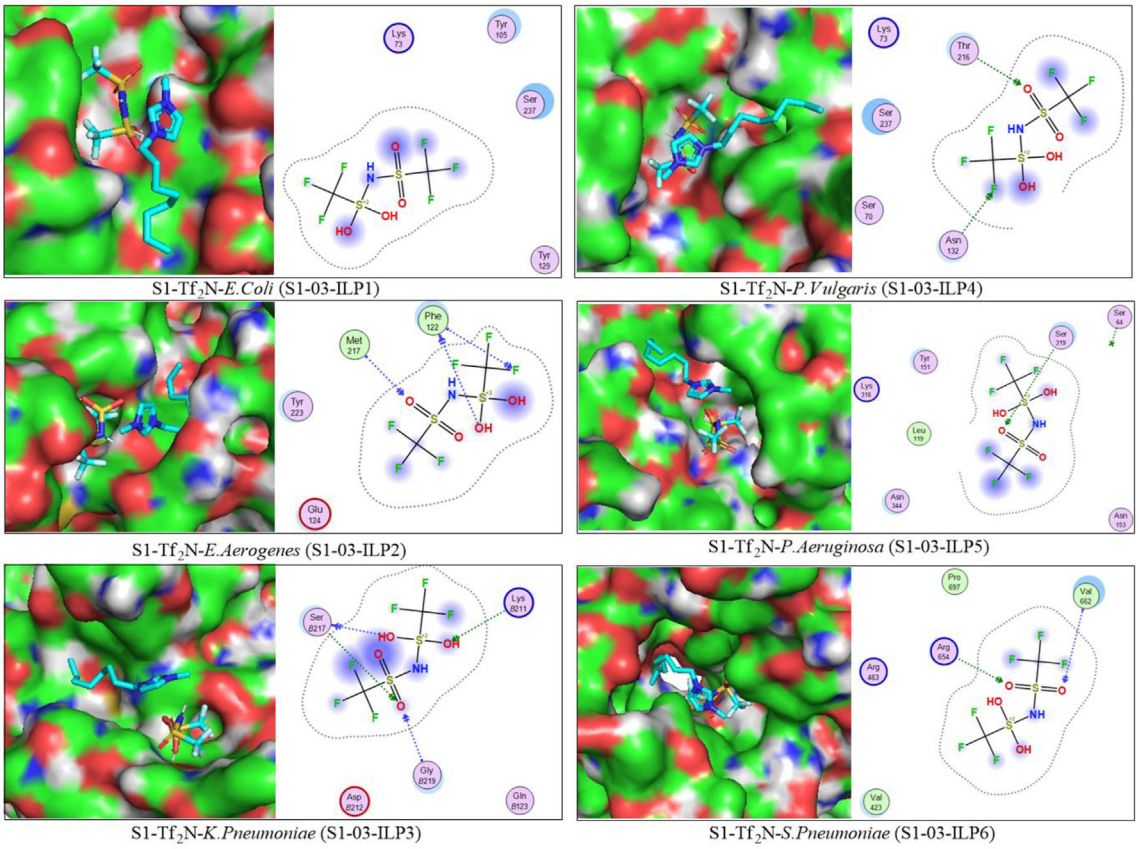


**Figure 4.** Molecular docking results of imidazolium-based IL S1-03 with bacteria.

strains like *E. aerogenes, P. vulgaris, K. pneumoniae, P. aeruginosa, E. coli, and S. pyogenes*.

The antibacterial activity of these synthesized ILs was evaluated by the diameter of the inhibition zone on agar plates. This zone is defined as an area on the plate where the growth of the bacteria was prevented.

The ILs based on octyl-imidazolium showed the highest antibacterial activity against all strains of the bacteria; some ILs were even more effective than positive control levofloxacin. Table 1 and Figure 1 show that the ILs based on octyl imidazolium were effective against all bacterial strains. The **IL S1-02** showed the highest inhibition values of 27 mm for *E. aerogenes* and 24 mm against *P. aeruginosa,* while **IL S1-06** showed no inhibition against *S. pneumoniae.* The ILs based on quaternary salts of pyridinium showed antibacterial activity against *E. aerogenes* and *K. pneumoniae.* It is clear from Figure 2 and Table 2 that **ILs S2-04 and S2-05** show the highest inhibition against *K. pneumoniae* with an IZ value of 20 mm Table 3 and Figure 3 show the bacterial inhibition for ILs based on quaternary salts of phosphonium with the highest IZ value of 14 mm against *E. aerogenes.* All phosphonium-based ILs also showed effectiveness against *E. coli.* Overall, all 18 synthesized ILs showed inhibition effectiveness, but ILs based on imidazolium are more effective than others. The order of effectiveness is as follows: ILs (Imidazolium) > ILs (phosphonium) ~ ILs (Pyridinium).

### 3.5. In-silico antibacterial activity

The antibacterial activity can also be analyzed using in-silico methods like Molecular Docking studies. The strong binding energy of ligand (drug or inhibitors) with the protein shows the maximum inhibition or higher antibacterial activity. Therefore, in this research, molecular docking studies were performed on all the 18 ionic liquids with the β-Lactamase protein of six bacteria; *E. coli* (PDB ID: 5A92), *E. aerogenes* (PDB ID: 5KID), *K. pneumonia* (PDB ID: 6MGX), *P. vulgaris* (PDB ID: 1HZO), *P. aeruginosa* (PDB ID: 4GZB), and *S. pneumoniae* (PDB ID: 1RPS). Details of the docking protocol are mentioned in the Computational details; however, docking results are presented in Table 4.

Molecular docking results for the imidazolium-based ionic liquids show that the IL **S1-01** shows potent inhibition with all the gram-positive and gram-negative bacteria's ranging binding affinity values from -6.3 to -7.7 kcal/mol. All the binding pockets and their interactions are presented in Table 5 and Figure 4.

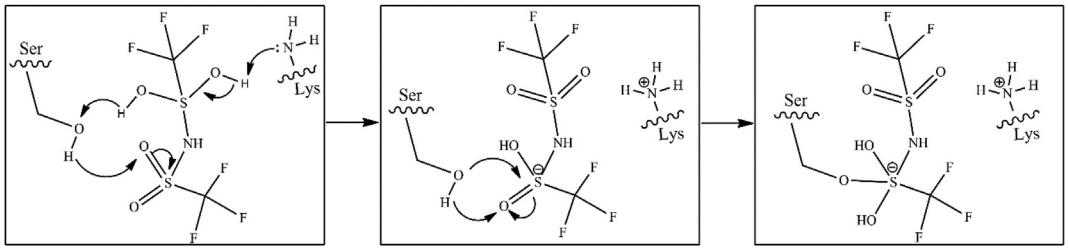


**Figure 5.** Proposed reaction mechanism for β-lactamase inhibition with S1-03.

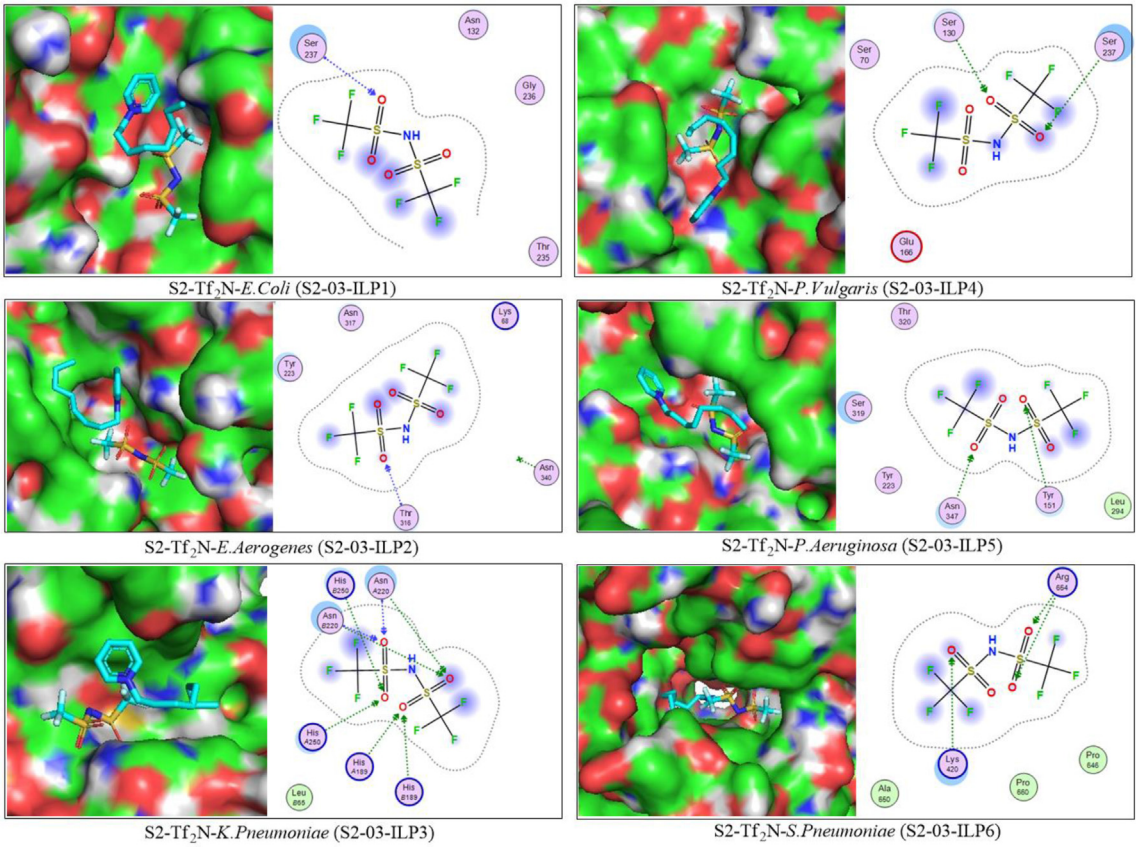


**Figure 6.** Molecular docking results of pyridinium-based ILs S2-03 with bacteria.

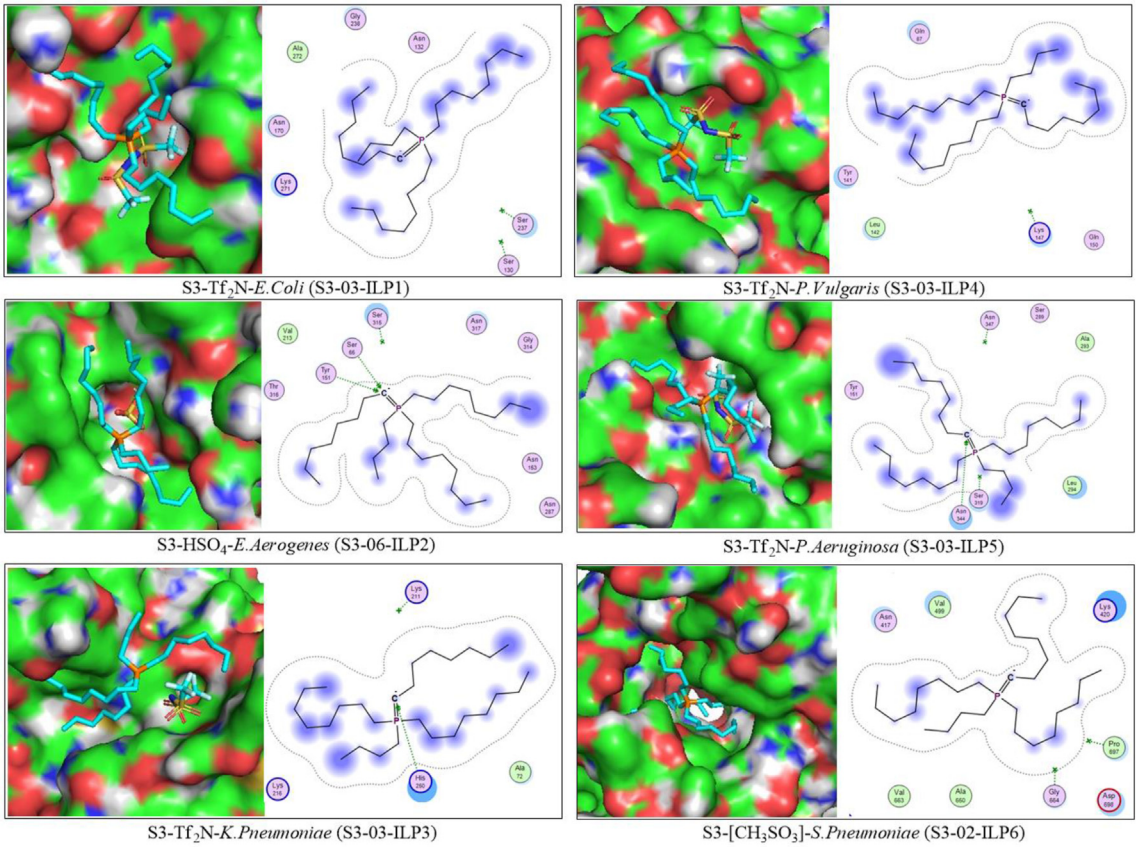


**Figure 7.** Molecular docking results of phosphonium-based ILs with bacteria.

The proposed reaction mechanism for inhibiting β-lactamase with IL **S1-03** is presented in Figure 5, showing the maximum inhibition capacity. It has been observed in Figure 4 (S1-03-ILP3) that Ser and Lys are present at the binding sight showing maximum interaction. According to the proposed reaction mechanism, the simultaneous transfer of protons occurs (Figure 5), resulting in the formation of positively charged Lys and direct bonding of Ser with the anion part of ionic liquid.

On comparing the docking results for the pyridinium-based ILs, the same behavior was observed as for imidazolium-based ILs. The IL **S2-03** shows the maximum inhibition with all the six bacteria with the binding affinity values ranging from -6.4 to -8.4 (Figure 6).

On the other hand, when the molecular docking results for phosphonium-based ionic liquids were analyzed, slightly different behavior was observed; the IL **S3-03** shows maximum inhibition for *E. coli, K. pneumonia, P. vulgaris,* and *P.* aeruginosa, however, **S3-06** shows maximum inhibition for *E. aerogenes* and **S3-02** shows maximum inhibition for S. *pneumonia* (Figure 7).

Analyzing the molecular docking results, it was also observed that the anionic part of imidazolium and pyridinium-based ILs interacts with the amino acids present at the active site; however, in the case of phosphonium based ILs, the cationic part of ILs shows interaction at the binding site. On comparing all the molecular docking results of the three schemes of imidazolium, pyridinium, and phosphonium-based ILs, it was observed that the pyridinium-based ILs would show strong binding affinity values and has maximum inhibition capacity relative to the other two schemes of ILs.

## 4. Conclusions

In brief, 18 ILs based on octyl pyridinium, octyl imidazolium, and mono-butyl-tri-octyl phosphonium cations and anions like bromide, sodium methane sulphonate, lithium bis(trifluoro-methane-sulfonyl)imide, sodium dichloroacetate, and sodium tetrafluoroborate, and potassium hydrogen sulfate were prepared as effective antibacterial agents. All the synthesized ILs were characterized by FTIR and NMR. The antibacterial activity of these ILs was tested by the agar well diffusion method against both gram-positive and gram-negative bacteria like *E. aerogenes, P. vulgaris, K. pneumoniae, P. aeruginosa, E. coli, and S. pyogenes.*

The ILs based on imidazolium showed the highest antibacterial activity against all tested bacteria and are more antibacterial than positive control levofloxacin. The IL **S1-02** showed the highest inhibition with an IZ value of 27 mm for *E. aerogenes* and 24 mm against *P. aeruginosa,* while IL **S1-06** showed no inhibition against *S. pneumoniae.* ILs based on pyridinium showed activity against *E. aerogenes and K. pneumoniae,* with ILs S2-04 and S2-05 showing the highest inhibition against *K. pneumoniae* with an IZ value of 20 mm. In contrast, the ILs based on phosphonium showed activity against *E. coli and E. aerogenes,* with the highest IZ value of 14 mm against *E. aerogenes.* The order of effectiveness is as follows: ILs (Imidazolium) > ILs (phosphonium) ~ ILs (Pyridinium). The molecular docking results show that IL **S1-03** shows potent inhibition with all bacteria with binding affinity values ranging from -6.3 to -7.7 kcal $mol^{-1}$. From pyridinium-based ILs, the IL **S2-03** shows the maximum inhibition with all the six bacteria with the binding affinity values ranging from -6.4 to -8.4 kcal $mol^{-1}$. While in the case of phosphonium-based ILs, the IL **S3-03** shows maximum inhibition for *E. coli, K. pneumonia, P. vulgaris,* and *P.* aeruginosa, however, **S3-06** shows maximum inhibition for *E. aerogenes* and **S3-02** shows maximum inhibition for S. *pneumonia.*

## Declarations

### Author contribution statement

Rabia Hassan: Conceived and designed the experiments; Performed the experiments; Analyzed and interpreted the data; Contributed reagents, materials, analysis tools or data; Wrote the paper.

Muhammad Asad Asghar, Arshemah Qaisar: Contributed reagents, materials, analysis tools or data; Wrote the paper.

Mudassir Iqbal: Conceived and designed the experiments; Analyzed and interpreted the data; Contributed reagents, materials, analysis tools or data; Wrote the paper.

Uzma Habib: Conceived and designed the experiments; Contributed reagents, materials, analysis tools or data; Wrote the paper.

Bashir Ahmad: Performed the experiments; Analyzed and interpreted the data.

### Funding statement

This research did not receive any specific grant from funding agencies in the public, commercial, or not-for-profit sectors and proceed further with the article.

### Data availability statement

Data included in article/supplementary material/referenced in article.

### Declaration of interests statement

The authors declare no conflict of interest.

### Additional information

No additional information is available for this paper.

## Acknowledgement

This work was supported by the School of Natural Sciences (SNS), National University of Sciences and Technology (NUST).

## References

[1] Z. Zheng, et al., Structure-antibacterial activity relationships of imidazolium-type ionic liquid monomers, poly(ionic liquids) and poly(ionic liquid) membranes: effect of alkyl chain length and cations, ACS Appl. Mater. Interfaces 8 (20) (2016) 12684–12692.
[2] W.H. Organization, Report on the Burden of Endemic Health Care-Associated Infection Worldwide, 2011.
[3] S. Gantz, A. Copeland, C.A. Zapka, Sanitizer Composition with Probiotic/prebiotic Active Ingredient, Google Patents, 2020.
[4] R.K. Chhetri, A. Baun, H.R. Andersen, Acute toxicity and risk evaluation of the CSO disinfectants performic acid, peracetic acid, chlorine dioxide and their by-products hydrogen peroxide and chlorite, Sci. Total Environ. 677 (2019) 1–8.
[5] F. Hitzenbichler, et al., Antibiotic resistance in E. coli isolates from patients with urinary tract infections presenting to the emergency department, Infection 46 (3) (2018) 325–331.
[6] M.A. Siddiquee, et al., In-vitro cytotoxicity, synergistic antibacterial activity and interaction studies of imidazolium-based ionic liquids with levofloxacin, J. Mol. Liq. (2021) 325.
[7] R. Patel, J. Saraswat, Effect of imidazolium-based ionic liquid on the antibacterial activity of an expired drug rifampicin, J. Mol. Liq. (2021).
[8] N. Nikfarjam, et al., Antimicrobial Ionic Liquid-Based Materials for Biomedical Applications, Advanced Functional Materials 31 (42) (2021).
[9] Ibsen, K.N., et al., *Mechanism of Antibacterial Activity of Choline-Based Ionic Liquids (CAGE)*. ACS Biomater Sci Eng, 2018. 4(7): p. 2370–2379
[10] T. Guo, et al., Effects of Alkyl Side-Chain Length on Binding with Bovine Serum Albumin, Cytotoxicity, and Antibacterial Properties of 1-Alkyl-3-Methylimidazolium Dicyanamide Ionic Liquids 339, 2021, p. 116835.
[11] W. Ochędzan-Siodłak, K. Dziubek, D. Siodłak, Densities and viscosities of imidazolium and pyridinium chloroaluminate ionic liquids, J. Mol. Liq. 177 (2013) 85–93.
[12] M.T. Garcia, et al., Aggregation behavior and antimicrobial activity of ester-functionalized imidazolium- and pyridinium-based ionic liquids in aqueous solution, Langmuir 29 (8) (2013) 2536–2545.
[13] M.T. Garcia, et al., Surface activity, self-aggregation and antimicrobial activity of catanionic mixtures of surface active imidazolium- or pyridinium-based ionic liquids and sodium bis(2-ethylhexyl) sulfosuccinate, J. Mol. Liq. (2020) 303.
[14] Y. Cao, T. Mu, Comprehensive investigation on the thermal stability of 66 ionic liquids by thermogravimetric analysis, Ind. Eng. Chem. Res. 53 (20) (2014) 8651–8664.

[15] C.G. Cassity, et al., Ionic liquids of superior thermal stability, J. Chem. Commun. 49 (69) (2013) 7590–7592.
[16] Y. Yu, et al., Multifunctional hydrogel based on ionic liquid with antibacterial performance, J. Mol. Liq. (2020) 299.
[17] K.N. Ibsen, et al., Mechanism of antibacterial activity of choline-based ionic liquids (CAGE), ACS Biomater. Sci. 4 (7) (2018) 2370–2379.
[18] A. Aljuhani, et al., Microwave-assisted synthesis of novel imidazolium, pyridinium and pyridazinium-based ionic liquids and/or salts and prediction of physico-chemical properties for their toxicity and antibacterial activity, J. Mol. Liq. 249 (2018) 747–753.
[19] G.R. Navale, M.S. Dharne, S.S. Shinde, Antibiofilm activity of tert-BuOH functionalized ionic liquids with methylsulfonate counteranions, RSC Adv. 5 (83) (2015) 68136–68142.
[20] G.K.K. Reddy, Y. Nancharaiah, V. Venugopalan, Long alkyl-chain imidazolium ionic liquids: antibiofilm activity against phototrophic biofilms, J. Colloid. Surf. B: Biointerfaces 155 (2017) 487–496.
[21] J.N. Pendleton, B.F. Gilmore, The antimicrobial potential of ionic liquids: a source of chemical diversity for infection and biofilm control, Int. J. Antimicrob. Agents 46 (2) (2015) 131–139.
[22] A.M. El-Shamy, et al., Anti-bacterial and anti-corrosion effects of the ionic liquid 1-butyl-1-methylpyrrolidinium trifluoromethylsulfonate, J. Mol. Liq. 211 (2015) 363–369.
[23] Z. Fallah, et al., Ionic liquid-based antimicrobial materials for water treatment, air filtration, food packaging and anticorrosion coatings, Adv. Colloid Interface Sci. 294 (2021) 102454.
[24] P.K. Mohapatra, et al., A novel CMPO-functionalized task specific ionic liquid: synthesis, extraction and spectroscopic investigations of actinide and lanthanide complexes, J. Dalton. Transact. 42 (13) (2013) 4343–4347.
[25] P.K. Mohapatra, et al., Diglycolamide-functionalized calix [4] arenes showing unusual complexation of actinide ions in room temperature ionic liquids: role of ligand structure, radiolytic stability, emission spectroscopy, and thermodynamic studies, J. Inorgan. Chem. 52 (5) (2013) 2533–2541.
[26] P.K. Mohapatra, et al., Highly efficient diglycolamide-based task-specific ionic liquids: synthesis, unusual extraction behaviour, irradiation, and fluorescence studies, J Chem. A Eur. J. 19 (9) (2013) 3230–3238.
[27] A. Sengupta, et al., Extraction of Am (III) using novel solvent systems containing a tripodal diglycolamide ligand in room temperature ionic liquids: a 'green'approach for radioactive waste processing, J RSC Adv. 2 (19) (2012) 7492–7500.
[28] A. Sengupta, et al., A diglycolamide-functionalized task specific ionic liquid (TSIL) for actinide extraction: solvent extraction, thermodynamics and radiolytic stability studies, J. Separ. Purific. Technol. 118 (2013) 264–270.
[29] A. Sengupta, et al., Studies on neptunium complexation with CMPO-and diglycolamide-functionalized ionic liquids: experimental and computational studies, J. New J. Chem. 41 (2) (2017) 836–844.
[30] T.T. Tran, et al., Synthesis of succinimide based ionic liquids and comparison of extraction behavior of Co (II) and Ni (II) with bi-functional ionic liquids synthesized by Aliquat 336 and organophosphorus acids, J. New J. Chem. 238 (2020) 116496.
[31] Z. Zhang, J. Song, B. Han, Catalytic transformation of lignocellulose into chemicals and fuel products in ionic liquids, Chem. Rev. 117 (10) (2017) 6834–6880.
[32] K.S. Egorova, E.G. Gordeev, V.P. Ananikov, Biological activity of ionic liquids and their application in pharmaceutics and medicine, Chem. Rev. 117 (10) (2017) 7132–7189.
[33] R.J.V. Ferraz, Development of Novel Active Pharmaceutical Ionic Liquids and Salts Based on Antibiotics and Anti-fungal Drugs, Repository, 2013.
[34] F. Endres, Physical chemistry of ionic liquids, Phys. Chem. Chem. Phys. 12 (8) (2010) 1648.
[35] Z. Zheng, et al., Structure–antibacterial activity relationships of imidazolium-type ionic liquid monomers, poly (ionic liquids) and poly (ionic liquid) membranes: effect of alkyl chain length and cations, JACS Appl. Mater. Interf. 8 (20) (2016) 12684–12692.
[36] H. Hajfarajollah, et al., Antibacterial and antiadhesive properties of butyl-methylimidazolium ionic liquids toward pathogenic bacteria, RSC Adv. 4 (80) (2014) 42751–42757.
[37] O. Forero Doria, et al., Novel alkylimidazolium ionic liquids as an antibacterial alternative to pathogens of the skin and soft tissue infections, Molecules 23 (9) (2018) 2354.
[38] A. Aljuhani, et al., Novel pyridinium based ionic liquids with amide tethers: microwave assisted synthesis, molecular docking and anticancer studies, J. Mol. Liq. 285 (2019) 790–802.
[39] A. Titi, et al., Novel phenethylimidazolium based ionic liquids: design, microwave synthesis, in-silico, modeling and biological evaluation studies, J. Mol. Liq. (2020) 315.
[40] N.S. Alahmadi, R.F.M. Elshaarawy, Novel aminothiazolyl-functionalized phosphonium ionic liquid as a scavenger for toxic metal ions from aqueous media; mining to useful antibiotic candidates, J. Mol. Liq. 281 (2019) 451–460.
[41] J. Cybulski, et al., Mandelate and prolinate ionic liquids: synthesis, characterization, catalytic and biological activity, Tetrahedron Lett. 52 (12) (2011) 1325–1328.
[42] S. Anvari, et al., Antibacterial and anti-adhesive properties of ionic liquids with various cationic and anionic heads toward pathogenic bacteria, J. Mol. Liq. 221 (2016) 685–690.
[43] T. Mehmood, M. Iqbal, R. Hassan, Prediction of Antibacterial Activity in Ionic Liquids through FTIR Spectroscopy with Selection of Wavenumber by PLS, 206, Chemometrics and Intelligent Laboratory Systems, 2020, p. 104124.
[44] C. Lee, W. Yang, R.G. Parr, Development of the Colle-Salvetti correlation-energy formula into a functional of the electron density, Phys. Rev. B Condens. Matter 37 (2) (1988) 785–789.
[45] S. Huzinaga, J. Andzelm, M. Klobukowski, E. Radzio-Andzelm, Y. Sakai, H. Tatewaki, I - general introduction, in: s. huzinaga (Ed.), Physical Sciences Data, Elsevier, 1984, pp. 1–11.
[46] J. Saraswat, P. Singh, R. Patel, A computational approach for the screening of potential antiviral compounds against SARS-CoV-2 protease: ionic liquid vs herbal and natural compounds, J. Mol. Liq. 326 (2021) 115298.
[47] J. Saraswat, et al., Noncovalent conjugates of ionic liquid with antibacterial peptide melittin: an efficient combination against bacterial cells, ACS Omega 5 (12) (2020) 6376–6388.
[48] J. Saraswat, et al., Synergistic antimicrobial activity of N-methyl substituted pyrrolidinium-based ionic liquids and melittin against Gram-positive and Gram-negative bacteria, Appl. Microbiol. Biotechnol. 104 (24) (2020) 10465–10479.
[49] al V G V e, Exploring the mechanism of β-lactam ring protonation in the class A β-lactamase acylation mechanism using neutron and X-ray crystallography, J. Med. Chem. 59 (2016) 474–479.
[50] I. Captain, et al., Engineered recognition of tetravalent zirconium and thorium by chelator-protein systems: toward flexible radiotherapy and imaging platforms, Inorg. Chem. 55 (2016) 11930–11936.
[51] Kim, Y., et al., *Crystal Structure Of the New Deli Metallo Beta Lactamase Variant 6 Klebsiella Pneumonia", to be published.*
[52] S.D.e.a. Lahiri, Structural insight into potent broad-spectrum inhibition with reversible recyclization mechanism: avibactam in complex with CTX-M-15 and Pseudomonas aeruginosa AmpC beta-lactamases, Antimicrob. Agents Chemother. 57 (6) (2013) 2496–2505.
[53] N.-L. Chan, et al., Crystallographic analysis of the interaction of nitric oxide with quaternary-T human haemoglobin, Biochemistry 43 (1) (2004) 118–132.
[54] M. Messali, et al., New eco-friendly 1-alkyl-3-(4-phenoxybutyl) imidazolium-based ionic liquids derivatives: a green ultrasound-assisted synthesis, characterization, antibacterial activity and POM analyses, Molecules 19 (8) (2014) 11741–11759.
[55] A. Cieniecka-Rosłonkiewicz, et al., Synthesis, anti-microbial activities and anti-electrostatic properties of phosphonium-based ionic liquids, Green Chem. 7 (12) (2005).
[56] J. Pernak, K. Sobaszkiewicz, I. Mirska, Anti-microbial activities of ionic liquids, Green Chem. 5 (1) (2003) 52–56.